Catalytic partial oxidation of methane on Ni-YSZ cermet anode of solid oxide fuel cells

Iwai, H.; Tada, K.; Kishimoto, M.; Saito, M.; Yoshida, H.

Catalytic partial oxidation of methane on Ni-YSZ cermet anode of solid oxide fuel cells

2016 J. Phys.: Conf. Ser. 745 032150

(http://iopscience.iop.org/1742-6596/745/3/032150)

7th European Thermal-Sciences Conference (Eurotherm2016) IOP Publishing
Journal of Physics: Conference Series **745** (2016) 032150 doi:10.1088/1742-6596/745/3/032150

Catalytic partial oxidation of methane on Ni-YSZ cermet anode of solid oxide fuel cells

H Iwai, K Tada, M Kishimoto, M Saito and H Yoshida

Department of Aeronautics and Astronautics, Kyoto University
Nishikyo-ku, Kyoto, 615 8540 Japan

E-mail: iwai.hiroshi.4x@kyoto-u.ac.jp

Abstract. The effects of oxygen addition to the methane fuels directly supplied to solid oxide fuel cells were investigated. Fundamental experiments were conducted using Ni-YSZ cermet as a typical anode material. The Ni-YSZ catalysts having different streamwise lengths were fabricated on the YSZ flat plates. Premixed gas of methane, oxygen, nitrogen and stream was supplied to the test catalyst set in a rectangular test channel. The exhaust gas compositions and the surface temperature distributions of the test catalyst were measured. It was found that the oxidation of methane prominently proceeded near the upstream edge of the catalyst followed by steam/dry reforming reactions downstream. It resulted in a formation of the high temperature region leading a large temperature gradient in the streamwise direction.

1. Introduction

The operating temperature of solid oxide fuel cells makes a good match with the temperature range of steam reforming reactions of hydrocarbon fuels. Heat generated in the SOFC systems can effectively be utilized in the endothermic reforming reactions. A reformer is usually placed next to the SOFC stack in many of the recent small SOFC systems so that the heat is transferred from the SOFC stack to the reformer [1][2]. This configuration is known as the indirect internal reforming.

There are investigations, on the other hand, on the direct internal reforming (DIR) [3][4]. In the DIR, the mixed gas of hydrocarbon and steam is directly supplied to the anode where the steam reforming reaction proceeds using nickel contained in the electrode as the reforming catalyst. A separate reformer is unnecessary in this configuration, which simplifies the system. Due to the strong endothermic nature of the reforming reaction, however, the cell temperature is often locally decreased near the inlet, resulting in a steep temperature gradient that may cause a cracking of the cells [5][6]. Similar difficulty is also found in the direct dry reforming of the biogas. As an idea to mitigate the cold spot caused by the endothermic reforming reactions, investigations on the effects of oxygen (air) addition to the fuel flow can be found in literature [7]. Some portion of the fuel is catalytically oxidized releasing heat to be utilized in the endothermic reforming reactions, which can level the temperature gradient along the cells.

Another example of such intentional oxygen supply to the SOFC anodes is the SOFCs operated under a single chamber mode (SC-SOFC) [8]–[10]. In the SC-SOFC, a premixed gas of the fuel and air is supplied to both electrodes. Shao [11] attached ruthenium catalyst on the anode of a small SC-SOFC and successfully demonstrated that the hydrogen generated by the catalytic partial oxidation of propane was effectively used in the power generation. However, excessive heat generation may become a problem if this method is applied to a cell with large electrode area.

Apart from the intentional addition of oxygen to the fuel, there is also a possibility of undesired inclusion of oxygen to the fuel flow due to unexpected failures in real systems. It may cause damages to the cells, affect durability of the system and raise safety problems.

Understanding the effects of oxygen addition to the hydrocarbon fuels in SOFC systems is important to establish a safe and reliable thermal management and to achieve long-term durability of the systems mentioned above. There are, however, few works on the phenomena occurring on the SOFC anodes under such conditions. In this study, we experimentally investigate the effects of oxygen addition to the hydrocarbon fuel supplied to SOFC anodes, to elucidate the fundamental characteristics of the anodes as catalyst for partial oxidation. Premixed gas of methane, oxygen, nitrogen and steam is supplied to the Ni-YSZ catalyst set in a rectangular test channel. The exhaust gas composition and the temperature distribution of the catalyst surface are measured.

2. Experiment

2.1. Catalytic partial oxidation

In this study, methane is used as fuel. The overall reaction of the catalytic partial oxidation of methane can be expressed as follows.

$$CH_4 + \frac{1}{2}O_2 = 2H_2 + CO \qquad \Delta H^0_{298} = -36\text{kJ / mol} \qquad (1)$$

When methane is directly converted into H_2 and CO as expressed in reaction (1) [12], it is called as "direct mechanism." On the other hand in the "indirect mechanism," the partial oxidation reaction is explained as a combination of the total oxidation, steam reforming reaction and dry reforming reaction expressed by reaction (2) – (4), respectively [13][14].

$$CH_4 + 2O_2 = 2H_2O + CO_2 \qquad \Delta H^0_{298} = -803\text{kJ / mol} \qquad (2)$$
$$CH_4 + H_2O = 3H_2 + CO \qquad \Delta H^0_{298} = 206\text{kJ / mol} \qquad (3)$$
$$CH_4 + CO_2 = 2H_2 + 2CO \qquad \Delta H^0_{298} = 248\text{kJ / mol} \qquad (4)$$

In the indirect mechanism, the reaction starts with the total oxidation of methane generating H_2O and CO_2. The generated H_2O and CO_2 are then consumed in the following steam reforming and dry reforming reactions to produce H_2 and CO. The water gas shift reaction expressed by reaction (5) also takes place.

$$CO + H_2O = CO_2 + H_2 \qquad \Delta H^0_{298} = -41\text{kJ / mol} \qquad (5)$$

In this paper we do not presume either of the two mechanisms mentioned above in the discussion. We start discussion considering all of the five reactions shown above as possible main reactions.

2.2. Sample preparation

We fabricated Ni-YSZ cermet (Ni :YSZ = 60 : 40 vol.%, YSZ: 8mol%Y_2O_3–ZrO_2) on a YSZ flat plate (width = 26mm, length = 70mm and thickness = 500μm) and used as test catalysts [15]. Note that Ni-YSZ cermet is a typical material for SOFC anodes. NiO powder and YSZ powder were mixed and ball-milled for 24 h with ethanol and zirconia balls (ϕ4.0 mm) to disperse the particles. After the milling, ethanol was evaporated using a hot stirrer at around 100 ºC, and the resultant powder was pre-sintered at 1400 ºC for 5 h. After that it was ground for 3 h and mixed with polyethylene glycol to form slurry. The slurry was screen-printed on the YSZ plate and sintered at 1400 ºC for 5 h. The test catalysts are approximately 26 mm width and 200μm thick. Three catalysts were prepared varying the streamwise length: 5, 10 and 30 mm. Figure 1 shows a picture of a test catalyst, whose streamwise length, L, is 30mm. Note that the catalysts need to be reduced before the experiments to convert NiO into Ni.

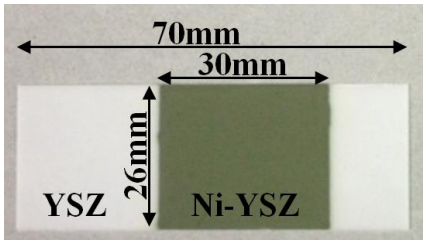

Figure 1. Ni-YSZ catalyst fabricated on a YSZ plate.

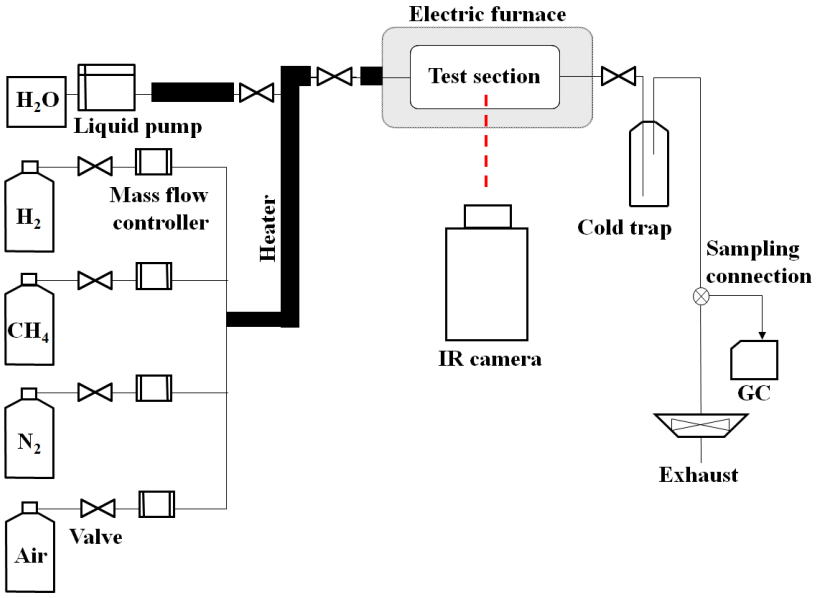

Figure 2. Schematic diagram of the experimental apparatus.

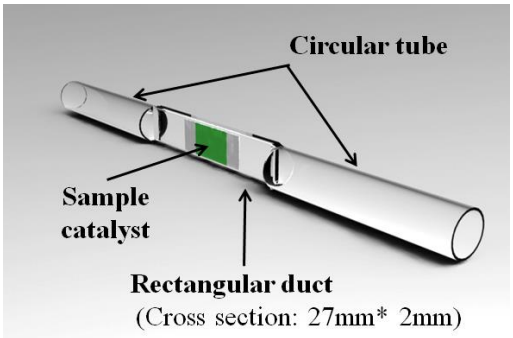

Figure 3. The test section with a sample plate.

2.3. Experimental apparatus

The experimental apparatus is schematically shown in figure 2. The mixture gas of methane, air (oxygen) and nitrogen is supplied to the test section. Hydrogen is used for the reduction of NiO at the beginning of the experiments. There is also a line for water vapor supply to see the effects of steam content in the supply gas. The gas flow rates are controlled using mass flow controllers with 1 % FS (100 sccm) accuracy. The accuracy of a liquid pump is 1% of the setpoint. The test section is placed in an electric furnace to control and maintain the high operating temperature. A part of the furnace is slightly opened in a rectangular shape at the catalyst position to measure the surface temperature distribution on the Ni-YSZ catalyst with an infrared (IR) camera. The exhaust gas composition is measured using a gas chromatograph (GC). Figure 3 shows the test section; it is a tube of quarts glass

having a rectangular cross section at the center part. The height and width of the rectangular cross section is 2 mm and 27 mm, respectively. The sample plate is placed in the center part as shown in the figure. The origin of the coordinate is set at the upstream edge of the Ni-YSZ catalyst. The *x*- direction corresponds to the streamwise direction.

The IR camera used in this study has a spectral range of 3.4 to 5.1 μm, which enables to measure the surface temperature of the Ni-YSZ through the quarts wall. The emissivity of the Ni-YSZ surface assumed in IR imaging is used as a tuning parameter so that the output of the IR measurement can reproduce the temperature measured by thermocouples attached on the Ni-YSZ catalyst. The emissivity is set at 0.98. The root mean square error of the IR measurements estimated based on the thermocouple measurements is 0.5 ºC in the temperature range of this study.

2.4. Experimental conditions

We introduce the mixing ratio, R_{mix}, which is defined as the molar ratio of CH_4 to that of O_2 in the supply gas. The stoichiometric values of R_{mix} for the total and partial oxidation of methane are 0.5 and 2.0, respectively. Inlet gas composition is varied to observe its effects on the catalytic reactions on the Ni-YSZ catalysts. The details of the inlet gas composition are explained for each experiment in the following chapter. The streamwise length of the Ni-YSZ catalyst, *L*, is varied in the range of 5 mm to 30 mm. The furnace temperature is set at 600 ºC throughout this study. The furnace temperature is measured with a monitoring thermocouple placed near the test section, but with a certain distance to avoid the effects of the reaction heat. When N_2 is supplied and no chemical reaction is occurring, the surface temperature was almost uniform at 589±1 ºC.

3. Results and discussion

In the following subsections 3.1 and 3.2, we discuss the effects of oxygen addition to the hydrocarbon fuel under dry condition. We supply the mixture gas of methane, oxygen and balance nitrogen to the test Ni-YSZ catalyst. The gas compositions set in the experiments are summarized in Table 1. The total flow rate is fixed at 220 ml/min. The flow rates of oxygen and nitrogen are varied while that of methane is kept constant resulting in the R_{mix} ranging from 0.6 to 1.2.

In the last subsection 3.3, we discuss the effects of steam addition to the supply gas. A pre-mixed gas of methane, oxygen, nitrogen and steam is supplied to the test catalyst. The experimental conditions are explained in the subsection 3.3.

Table. 1. Compositions of the supply gas.

	R_{mix}	0.6	0.7	0.8	0.9	1.0	1.1	1.2
Molar fraction at the inlet	O_2	0.19	0.16	0.14	0.12	0.11	0.10	0.09
	N_2	0.70	0.73	0.75	0.76	0.78	0.79	0.80
	CH_4	0.11	0.11	0.11	0.11	0.11	0.11	0.11

3.1. Activity of the catalyst

The Ni-YSZ catalysts are confirmed to be active and stable under most of the experimental conditions in this study. Figure 4 shows a typical example of the surface temperature distributions measured by the IR camera. The catalyst area is marked with dashed lines. The gas flows left to right. A high temperature zone is clearly formed near the upstream edge of the catalyst where the exothermic oxidation reaction is expected to be most active. As the temperature distribution is almost uniform in the spanwise direction except for the region near the sidewalls, we can confirm that the sidewall effects on the experimental data are not significant. It is found through the GC analysis that the exhaust gas contains nitrogen, methane, hydrogen, steam, CO and CO_2, but no oxygen, when the catalytic reactions reach a steady condition.

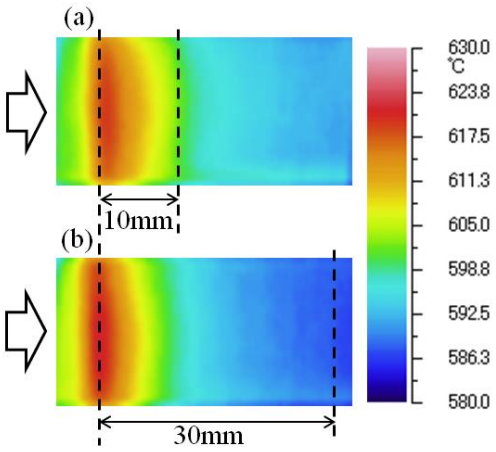

Figure 4. Surface temperature distribution on the test catalyst, R_{mix} = 1.2, (a) L = 10mm (b) L = 30 mm.

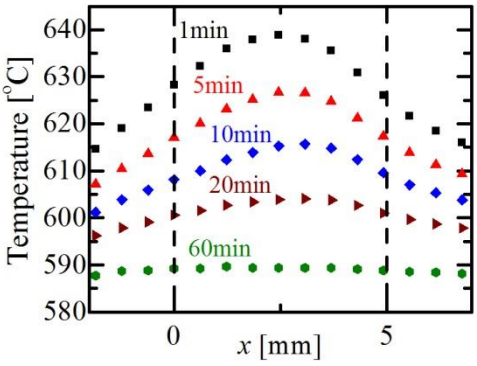

Figure 5. Evolution of the surface temperature distribution along the centerline, R_{mix}=0.7, L = 5mm.

When L = 5mm, the catalytic activity is lost under the conditions of R_{mix} = 0.6 and 0.7. Figure 5 shows an example of the time evolution of the surface temperature of the catalyst along the centerline for R_{mix} = 0.7. The catalyst is active at the beginning of the experiment when the reactive gas is started to be supplied. However, it gradually loses its activity and eventually no reaction is observed and the exhaust gas composition becomes same as that of the supply gas. The activity is lost because Ni in the catalyst is fully oxidized into NiO. Its activity recovers if the NiO reduction is performed again by supplying hydrogen. It is worth noting that during the deactivation process of the catalyst, the exhaust gas contains only nitrogen, methane, steam, oxygen and CO_2, but no hydrogen nor CO. It indicates that the total oxidation of methane occurs during this process, supporting the indirect mechanism for the partial oxidation of methane on a Ni-YSZ catalyst.

3.2. Effects of R_{mix} and catalyst length

The local temperature distributions along the centerline of the catalyst surface are presented in figure 6 for the three catalysts with different streamwise length. The mixing ratio, R_{mix}, is varied in the range of 0.6 to 1.2. Because the catalytic activity is lost in the cases of R_{mix} = 0.6 and 0.7 when L = 5 mm as explained above, the results for those conditions are not shown in the figure. The figure includes only the conditions under which stable reactions are observed. It clearly shows that a high temperature region is formed near the upstream edge of the catalyst. It indicates the exothermic oxidation reaction is active in that region. It is also supported by the facts that the area of the high temperature region is wider and the magnitude of the maximum temperature is higher for the lower R_{mix}.

By comparing the results of the three catalysts with different streamwise length, it is found that the surface temperature distributions of the three catalysts show little difference to each other when the supply gas composition is same. It indicates that the reactions occurring in the upstream region are not significantly affected by the downstream conditions. In the following discussion, we assume that the gas compositions at x = 5 and 10 mm in the case of L = 30 mm can be represented by the exhaust gas composition observed with L = 5 mm and 10 mm catalyst, respectively.

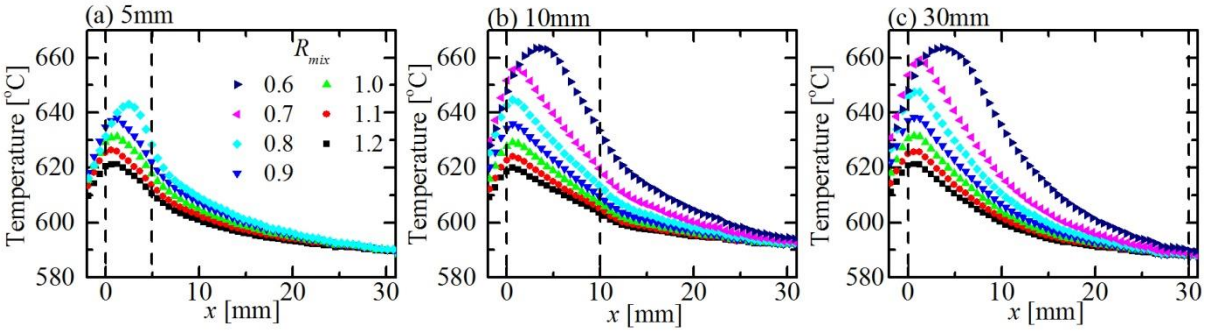

Figure 6. Local temperature distributions along the centerline at different R_{mix}.

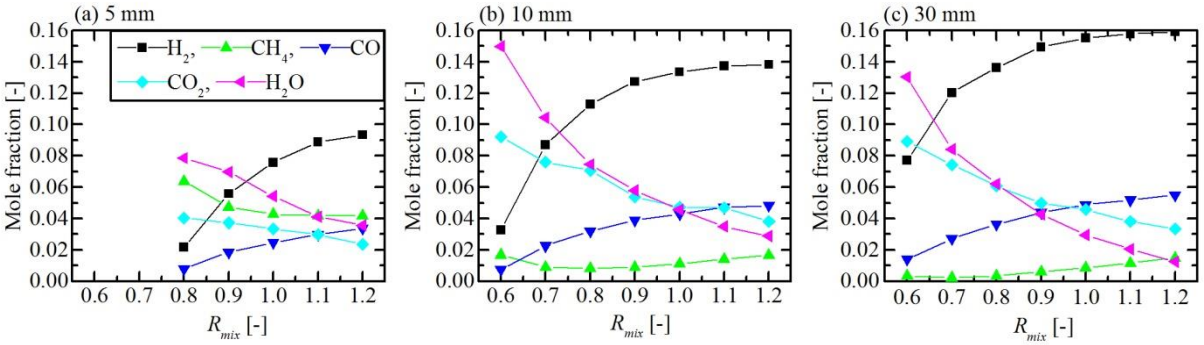

Figure 7. Exhaust gas composition.

Figure 7 shows the exhaust gas composition corresponding to the experiments shown in figure 6. Note that the molar fractions of steam shown in the figure are not measured values but calculated ones because steam is removed by a cold trap and cannot directly be measured by GC. Nitrogen is excluded because it does not participate in the reaction. Oxygen does not appear in the figure because it is completely consumed by the methane oxidation reaction. It can be observed in the figure that when R_{mix} is low the exhaust gas contains more CO_2 and H_2O than H_2 and CO, showing that the overall reaction is close to the total oxidation expressed by eq. (2). The molar fractions of H_2 and CO increase with an increase of R_{mix}, while that of CO_2 and H_2O show an opposite trend. The generation of H_2 and CO while consuming CO_2 and H_2O under relatively high R_{mix} conditions is attributed to steam/dry reforming of methane. It is consistent with the discussion in the subsection 3.1 supporting the indirect mechanism. The increasing or decreasing trends are clear but become moderate under the conditions of $R_{mix} > 0.9$.

Although figure 7 gives general trend of the reactions, quantitative discussion is difficult because the total molar flow rate is not constant in the experiments due to the reactions. The carbon selectivity in the exhaust gas is calculated and presented in figure 8 to develop a quantitative discussion. Note that the amount of methane in the supply gas is kept constant (Table 1). As the catalyst length increases, the remaining CH_4 in the exhaust gas decreases. The difference between the L = 5 mm and L = 10 mm is much larger than that between L =10mm and L = 30 mm. It indicates that the methane consumption is particularly fast within 10 mm from the upstream edge while it is moderate in the downstream region (10 mm < x < 30 mm). Combined with the fact that the supplied oxygen is completely consumed even in the cases of L = 5 mm, it is reasonable to judge that the prominent peak of the local temperature in figure 6 is a result of the exothermic oxidation followed by the endothermic reforming reaction occurring in a small region. As shown in figure 6, it results in a steep temperature gradient in this region. After the depletion of oxygen, the consumption of CH_4 is ascribed to the steam/dry reforming reactions. The increase of CO selectivity and decrease of CO_2 selectivity with an

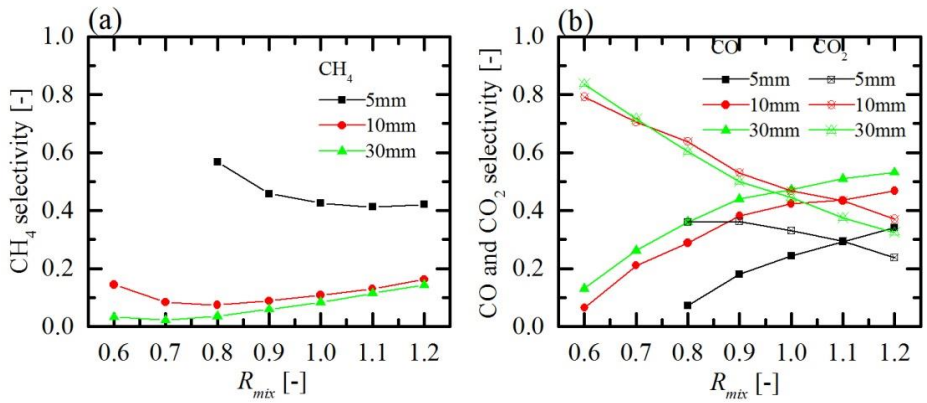

Figure 8. Effects of R_{mix} on carbon selectivity, (a) CH_4 selectivity (b) CO and CO_2 selectivity.

Table. 2. Effects of steam addition on the methane consumption, Total flow rate : 200ml/min.

	R_{mix}	1.5 dry	1.5	2.0	2.5
Molar fraction at the inlet	O_2	0.10	0.10	0.08	0.08
	N_2	0.75	0.45	0.45	0.41
	CH_4	0.15	0.15	0.17	0.21
	H_2O	0.00	0.30	0.30	0.30
Total consumption, ml/min (Consumption by reforming reaction)		22.3 (12.3)	23.7 (13.7)	23.2 (15.2)	26.1 (18.1)
Consumption rate, %		74.3	79.0	69.1	62.1

increase of R_{mix} at the high R_{mix} region can be explained by the water gas shift reaction. At the high R_{mix} region, the amount of remaining CH_4 in the exhaust gas is relatively high. Addition of steam/CO_2 to the supply gas may enhance the steam/dry reforming at the downstream region.

3.3. Influence of steam addition to the inlet gas

In the above subsections, the supply gas is kept dry at the inlet. In that case, the steam/dry reforming reactions are possible only after some portion of methane is oxidized producing steam and CO_2. In this subsection, we examine the effects of steam addition to the inlet gas. Methane, oxygen, nitrogen and steam are pre-mixed and supplied to the catalyst of L = 30 mm. R_{mix} is set higher than the previous subsections expecting that the effects of reforming reaction can clearly be observed. The total flow rate is kept constant at 200 ml/min. The experimental conditions and methane consumptions are summarized in table 2. Note that the methane consumption by the reforming reaction is calculated value from the experimental results assuming the indirect mechanism. The two cases at R_{mix} = 1.5 compare the conditions with and without steam in the supply gas. It shows that steam addition to the inlet gas enhances the methane consumption by the steam reforming reaction but its impact is moderate. When we compare the three cases with steam addition, R_{mix} = 1.5, 2.0 and 2.5, the methane consumed by the

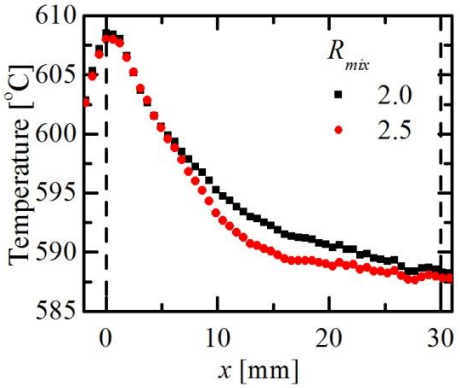

Figure 9. Local temperature distribution along the cneterline.

steam reforming reaction increases with an increase of methane supply. Local temperature distributions along the centerline are shown in figure 9 for R_{mix} = 2.0 and 2.5. Because the oxygen supply is same in these two cases, the peak temperature at the upstream edge of the catalyst is almost same. It also indicates that methane oxidation first occur even when sufficient steam for the reforming reaction is contained in the supply gas. A clear difference is observed in the downstream region around $10 < x < 20$ mm. Local temperature is lower for the case of R_{mix} = 2.5 caused by the enhanced reforming reaction.

4. Conclusions

We experimentally investigated the effects of oxygen addition to the hydrocarbon fuel supplied to SOFC anodes, to elucidate the fundamental characteristics of anodes as a catalyst for the partial oxidation reaction. Premixed gas of methane, oxygen, nitrogen and steam was supplied to the Ni-YSZ cermet anode set in a rectangular test channel. The exhaust gas composition and the surface temperature distributions of the test catalysts were measured.

(1) Ni-YSZ cermet anode is active for partial oxidation of methane. The experimental data supports the indirect mechanism; the reaction starts with the total oxidation of methane and generated H_2O and CO_2 are then consumed in the following steam/dry reforming reactions to produce H_2 and CO. Because of the strong exothermic nature of the total oxidation, a high temperature zone is formed near the upstream edge of the catalyst.

(2) Supplied oxygen is completely consumed within 5 mm from the upstream edge of the catalyst. Methane consumption by the oxidation and reforming is particularly active within 10 mm from the upstream edge. It forms a prominent peak of the local temperature resulting in the steep temperature gradient in the streamwise direction particularly under low R_{mix} conditions

(3) Methane oxidation reaction proceeds first even when the supply gas contains sufficient steam for the steam reforming reaction. Steam addition to the supply gas enhances the steam reforming reaction in the downstream region but has little influence on the oxidation reaction in the upstream region.

References

[1] Aguiar P, Chadwick D and Kershenbaum L 2002 *Chemical Engineering Science* **57** 1665–1677
[2] Brus G., 2012 *International Journal of Hydrogen Energy* **37** 17225–17234
[3] Achenbach E, Riensche E 1994 *Journal of Power Sources* **52** 283–288
[4] Achenbach E 1994 *Journal of Power Sources* **49** 333–348
[5] Iwai H, Yamamoto Y, Saito M and Yoshida H 2011 *Energy* **36** 2225–2234
[6] Wongchanapai S, Iwai H, Saito M and Yoshida H 2012 *Journal of Power Sources* **204** 14–24
[7] Shiratori Y, Tran T Q, Takahashi Y and Sasaki K. 2011 *ECS Transactions* **35** 2641–2651
[8] Hibino T, Hashimoto A, Yano M, Suzuki M and Sano M 2003 *Electrochimica Acta* **48** 2531–2537
[9] Yano M, Tomita A, Sano M and Hibino T 2007 *Solid State Ionics* **177** 3351–3359
[10] Riess I, 2008 *Journal of Power Sources* **175** 325–337
[11] Shao Z, Haile S M, Ahn J, Ronney P D, Zhan Z and Barnett S A, 2005, *Nature* **435** 795–798
[12] Hu Y H and Ruckenstein E 1996 *Journal of Catalysis* **158** 260–266
[13] Vermeiren W J M, Blomsma E and Jacobs P A 1992 *Catalysis today* **13** 427–436
[14] Smith M W, Shekhawat D 2011 Catalytic partial oxidation, *Fuel Cells: Technologies for fuel processing* ed D Shekhawat, J J Spivey, D A Berry, (Amsterdam: Elsevier) chapter 5 pp. 74–128
[15] Kishimoto M, Iwai H, Saito M and Yoshida H 2012 *Journal of The Electrochemical Society* **159** B315–B323